CHEMISTRY OF MATERIALS

ARTICLE

pubs.acs.org/cm

High-Resolution Synchrotron Studies and Magnetic Properties of Frustrated Antiferromagnets MAl_2S_4 ($M = Mn^{2+}$, Fe^{2+}, Co^{2+})

Melissa C. Menard,[†] Rieko Ishii,[‡] Tomoya Higo,[‡] Eigi Nishibori,[§] Hiroshi Sawa,[§] Satoru Nakatsuji,[‡] and Julia Y. Chan[†,*]

[†]Department of Chemistry, Louisiana State University, Baton Rouge, Louisiana 70803, United States

[‡]Institute for Solid State Physics, University of Tokyo, Kashiwa 277-8581, Japan

[§]Department of Applied Physics, Graduate School of Engineering, Nagoya University, Nagoya 464-8603, Japan

Supporting Information

ABSTRACT: Single crystals of MAl_2S_4 ($M = Mn^{2+}$, Fe^{2+}, Co^{2+}) were synthesized using the chemical vapor transport method and characterized using high-resolution synchrotron X-ray diffraction to determine the structure. All the compounds have a layered slab structure separated by a van der Waals gap, which results in highly two-dimensional magnetism. Magnetic susceptibility measurements indicate spin-glass behavior below T^* values of ~2 K, ~ 10.5 K, and ~5 K for MAl_2S_4 ($M = Mn^{2+}$, Fe^{2+}, Co^{2+}), respectively, and heat capacity measurements indicate no long-range magnetic ordering observed down to 0.4 K. These results can be attributed primarily to site disorder due to mixing of M^{2+} and Al^{3+} ions ($M = Mn^{2+}$, Fe^{2+}, Co^{2+}) and low dimensionality with geometrical frustration also playing a role. Interestingly, $MnAl_2S_4$, with almost isotropic $S = {}^5/_2$ spin, has the highest frustration parameter among the series of compounds and is a possible candidate for a two-dimensional Heisenberg spin glass system.

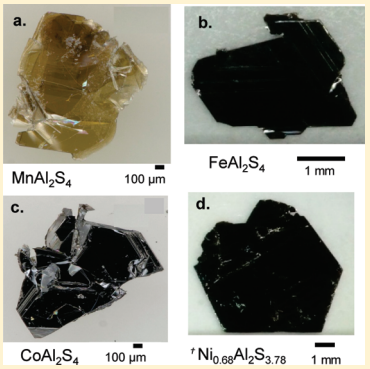

KEYWORDS: magnetism, disorder, dimensionality, geometrical frustration

INTRODUCTION

Primary interest in two-dimensional (2-d) triangular lattice antiferromagnets arises from the inherent lattice frustration, resulting in the suppression of long-range magnetic order to temperatures much lower than expected, because of competing interactions between magnetic moments.[1−4] The combination of frustration and 2-d magnetism can suppress magnetic ordering and allow for the investigation of the quantum fluctuations that determine the possible ground states of the system.[5] Quantum fluctuations are low-temperature phenomena with fingerprints evident on room-temperature physical properties. Understanding these ground states is critical for understanding the behavior at application temperatures and can lead to the design of new, exotic materials.[6,7]

Frustration when coupled with complex parameters such as the charge, spin, orbital, and lattice can lead to exotic phenomena and ground states. Various polytypes of the $ZnIn_2S_4$ structure type have been investigated because of the possible geometric frustration of magnetic moments on a triangular lattice. The $CuIr_2S_4$ and $MgTi_2O_4$ phases form spin dimers and have been correlated to charge ordering and frustration.[8,9] $FeSc_2S_4$, which is a spin−orbital liquid with one of the largest spin-frustration parameters > 900, exhibits complex spin−orbital coupling, in addition to frustration.[10] Electric polarization induced by an external magnetic field in $CdCr_2S_4$ and $HgCr_2S_4$ appears with and without complex spiral magnetic ordering, respectively.[11,12] Many spinels have been studied with various properties, because of geometrical frustration of the magnetic sublattice. Structurally related to the spinel structure type, $FeGa_2S_4$-type[13] and $ZnIn_2S_4$-type[14] compounds are good candidates for the investigation of quantum fluctuations, given the two dimensionality of the structure, in addition to the triangular magnetic sublattice. Although the Ga-analogues, MGa_2S_4 ($M = Mn^{2+}$, Fe^{2+}, Co^{2+}), adopt one of the $ZnIn_2S_4$ polytypes, previous attempts to grow the MAl_2S_4 ($M = Mn^{2+}$, Fe^{2+}, Co^{2+}) have failed, reportedly because of the polarizing capacity of Al^{3+} in these compounds to induce structural instability in the sulfide lattice, which results in the formation of a different structure.[15]

The layered $NiGa_2S_4$ ($FeGa_2S_4$-type) structure is the first reported example of a low-spin quasi-two-dimensional (quasi-2-d) antiferromagnet with a perfect triangular lattice.[4] Very interestingly, the Ni^{2+} ($S = 1$) spins do not show any long-range magnetic ordering down to 30 mK, despite the relatively large antiferromagnetic Weiss temperature (~80 K). Instead, the Ni^{2+} spins exhibit spin glass freezing at $T^* = 8.5$ K and show a 2-d spin wave-like coherent behavior at $T < 3$ K.[7] Spin-dependent impurity effects in $Ni_{1-x}M_xGa_2S_4$ ($M = Mn^{2+}$, Fe^{2+}, Co^{2+}, and Zn^{2+}) indicate that the integer size of the Heisenberg spins is important to stabilize the 2-d spin wave-like coherent behavior.[16] The high-spin ($S = 2$) $FeGa_2S_4$ has been described as a frustrated ($\theta = -160$ K) quasi-2-d triangular Heisenberg antiferromagnet exhibiting strong spin freezing at 16 K without developing magnetic long-range order.[13,17−20]

Received: February 23, 2011
Revised: May 13, 2011
Published: May 31, 2011

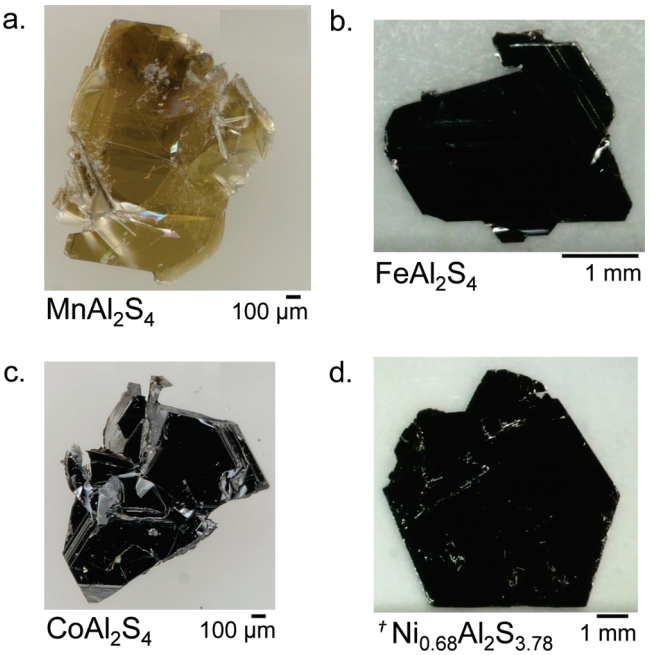

Figure 1. Single crystals of MAl_2S_4 (M = Mn^{2+}, Fe^{2+}, Co^{2+}) and $Ni_{0.68}Al_2S_{3.78}$.

Various polytypes of $CoGa_2S_4$ and $MnGa_2S_4$ have been reported, but not of the $FeGa_2S_4$ or $ZnIn_2S_4$ (IIIa) types.[21−24]

In addition to geometrical frustration, magnetic frustration can arise because of site disorder, as observed in the spinel-type $CoAl_{2-x}Ga_xO_4$, where doping of Ga^{3+} at both the octahedral and tetrahedral sites results in an increasingly diluted magnetic sublattice at concentrations of $0.4 \leq x \leq 2.0$.[25,26] Here, we report the growth and characterization of single crystals of MAl_2S_4 (M = Mn^{2+}, Fe^{2+}, Co^{2+}), which exhibit magnetic dilution due to mixing of M^{2+} (M^{2+} = Mn^{2+}, Fe^{2+}, Co^{2+}) and Al^{3+} in two interpenetrating, triangular magnetic sublattices, to investigate the effects of spin on structurally similar systems exhibiting magnetic frustration and the site disorder effects due to mixing on crystal chemistry and physical properties. Structural and magnetic comparison between MGa_2S_4 (M = Fe^{2+}, Ni^{2+}) and MAl_2S_4 (M = Mn^{2+}, Fe^{2+}, Co^{2+}) can be used to isolate the effects of low dimensionality and geometrical frustration from effects of site disorder.

EXPERIMENTAL SECTION

Synthesis. Polycrystalline samples of MAl_2S_4 (M = Mn^{2+}, Fe^{2+}, Co^{2+}) were synthesized by annealing M (M = Mn, Fe, Co) with Al and S in evacuated quartz ampules for 1−2 days at 900 °C. Single crystals were prepared by the chemical vapor transport (CVT) method in evacuated quartz ampules, using the polycrystalline samples obtained by the above procedure. The transport reactions were carried out in a temperature gradient of 850−950 °C for 1−2 weeks using a transport agent concentration of 3 mg/cm^3 iodine. Crystals, shown in Figure 1, grew as dark brown (light brown for $MnAl_2S_4$), hexagonal, micaceous plates and cleave easily. The crystals are very hygroscopic and react readily with water in the surrounding air to yield Al_2O_3, MS (M = Mn^{2+}, Fe^{2+}, Co^{2+}), and H_2S. The distinct smell of H_2S is indicative of crystal degradation.

Elemental Analysis. Scanning electron microscopy with energy-dispersive X-ray (SEM-EDX) measurements were performed to confirm the exact composition of MAl_2S_4 (M = Mn^{2+}, Fe^{2+}, Co^{2+}). Measurements were collected on a JEOL Model JSM-5600 instrument. The accelerating voltage was 15 kV, with a beam-to-sample distance of 20 mm. An average of 10 scans with a size of 10 μm × 10 μm was performed on each single crystal. The mole ratio of M:Al:S, normalized to an Al concentration of 2 mol, was obtained by fitting intensity as a function of energy to yield $Mn_{0.99(1)}Al_2S_{4.07(1)}$, $Fe_{0.92(1)}Al_2S_{3.97(1)}$, and $Co_{0.97(1)}Al_2S_{4.02(1)}$, which are consistent with the refined compositions determined by X-ray diffraction (XRD).

Single Crystal X-ray Diffraction. Data collection on single crystals using an Enraf Nonius diffractometer that was equipped with a Kappa CCD detector (Mo Kα radiation, λ = 0.71703 Å) was attempted on several crystals with long scan times. Since the single crystals were weakly diffracting, synchrotron crystallographic data were collected at the Advanced Light Source Synchrotron facility in Berkeley California at the Small-Crystal Crystallography Beamline 11.3.1 (Lawrence Berkeley National Laboratory). Intensity data were collected at 150 K on a D8 goniostat equipped with a Bruker APEXII CCD detector using synchrotron radiation tuned to λ = 0.7749 Å. A series of 1 s frames measured at 0.2° increments of ω were collected to calculate a unit cell. Data collection frames were measured for a duration of 1 s at 0.3° intervals of ω with a maximum 2θ value of ∼60°. The data were collected using the program APEX2[27] and processed using the SAINT[27] routine within APEX2. The data were corrected for absorption and beam corrections, based on the multiscan technique, as implemented in SADABS.[28] Direct methods were used to solve the structures,[29] and the models were refined using SHELX97[30] with extinction coefficients and anisotropic displacement parameters.

Refinement of MAl_2S_4 (M = Mn, Fe, Co). Crystallographic data, atomic positions, and bond distances for all compounds studied are provided in Tables 1, 2, and 3, respectively. Because of similar lattice parameters, the atomic positions of the hexagonal polymorph of $ZnIn_2S_4$ (IIIa)[14] were used as an initial structural model in determining the atomic positions of $MnAl_2S_4$, and the atomic positions of $FeGa_2S_4$[13] were used as an initial structural model in determining the atomic positions of both $FeAl_2S_4$ and $CoAl_2S_4$. Refinement of the models of MAl_2S_4 (M = Mn, Fe, Co), prior to mixing between M^{2+} and Al^{3+} at both the tetrahedral and octahedral sites, led to anomalous atomic displacement parameters at the octahedral and tetrahedral sites and high residuals of $\rho_{max} \approx 14.0$, $\rho_{min} \approx -3.0$, and R_1 = 13.5% for $MnAl_2S_4$, $\rho_{max} \approx 1.4$, $\rho_{min} \approx -0.7$, and $R_1 \sim 0.11$ for $FeAl_2S_4$, and $\rho_{max} \approx 3.7$, $\rho_{min} \approx -1.8$, and $R_1 \approx 0.16$ for $CoAl_2S_4$. Mixing of M^{2+} (M^{2+} = Mn, Fe, Co) and Al^{3+} at both the octahedral and tetrahedral sites resulted in smooth difference maps and overall lower residuals. The refined compositions of MAl_2S_4 (M = Mn, Fe, Co) are consistent with those determined by SEM-EDX analysis. No missing symmetry was found using PLATON.[31]

The models of $MnAl_2S_4$ and $CoAl_2S_4$ were both refined as twins. $MnAl_2S_4$ adopts a noncentrosymmetric space group ($R3m$) and is an inversion twin with a ∼7.2% contribution from the inverted component. The initial refinement of the model of $CoAl_2S_4$, using fully occupied atomic positions, resulted in reasonable atomic displacement parameters and values of the goodness of fit (GoF) parameter, but the residual value (R_1) remained ∼25% with unusually large residual electron density peaks ($\rho_{max} \approx 14$ and $\rho_{min} \approx -6$) that could not be resolved as disorder. Since the observed intensities (F_{obs}^2) for the most disagreeable reflections were symmetrically much greater than the calculated intensities (F_{calc}^2), the possibility of twinning was explored. The model of $CoAl_2S_4$ was refined with the twin law for trigonal, merohedral twinning (−1 0 0 0 −1 0 0 0 1) with a 34.6%:65.4% distribution from the two twin components and a R_1 value of ∼0.05.

Magnetic and Thermal Properties. Magnetization down to 2 K was measured under magnetic fields up to 9 T with a Quantum Design MPMS SQUID magnetometer to investigate the magnetic properties of MAl_2S_4 (M = Mn^{2+}, Fe^{2+}, Co^{2+}). The specific heat (C_p) was measured by the thermal relaxation method, down to 0.4 K,

dx.doi.org/10.1021/cm200561p |Chem. Mater. 2011, 23, 3086–3094

Table 1. Crystallographic Data of MAl_2S_4 (M = Mn^{2+}, Fe^{2+}, Co^{2+}, Ni^{2+}[a])

Crystal Data				
refined composition	$MnAl_2S_4$	$FeAl_2S_4$	$CoAl_2S_4$	$Ni_{0.68}Al_2S_{3.78}$
space group	$R3m$	$P\bar{3}m1$	$P\bar{3}m1$	$P\bar{3}m1$
a (Å)	3.7013(13)	3.6825(13)	3.6200(13)	3.6060(13)
c (Å)	36.4160(12)	12.1920(12)	11.9700(12)	11.9850(12)
V (Å^3)	432.1(2)	143.18(7)	135.84(7)	134.96(7)
Z	1	1	1	1
crystal size (mm^3)	0.01 × 0.04 × 0.10	0.02 × 0.04 × 0.005	0.01 × 0.03 × 0.04	0.02 × 0.11 × 0.14
Data Collection				
temperature (K)	150(2)	150(2)	150(2)	150(2)
measured reflections	1071	1506	1420	1296
independent reflections	283	148	141	140
reflections with I > 2σ(I)	272	113	141	136
R_{int}	0.0420	0.1238	0.0477	0.0267
h	−4 → 4	−4 → 4	−4 → 4	−4 → 4
k	−4 → 4	−4 → 4	−4 → 4	−4 → 4
l	−43 → 44	−14 → 14	−14 → 14	−14 → 14
Refinement				
θ range (°)	3.66−28.95	3.64−28.92	3.71−28.99	5.10−26.35
$R_1[F^2 > 2\sigma F^2)]$[b]	0.0210	0.0566	0.0285	0.0616
$wR_2(F^2)$[c]	0.0513	0.1262	0.0533	0.1484
number of parameters	23	13	16	13
goodness of fit, GoF on F^2	1.021	1.134	1.129	1.256
μ (mm^{-1})	4.150	5.371	5.965	4.132
Δp_{max} (e Å^{-3})	0.242	1.368	0.563	2.111
Δp_{min} (e Å^{-3})	−0.377	−0.669	−0.798	−1.795
extinction coefficient	0.00	0.47(9)	0.00	0.28(7)

[a] $NiAl_2S_4$ = $Ni_{0.68}Al_2S_{3.78}$. Data taken from ref 32. [b] $R_1 = \Sigma||F_0| - |F_c||/\Sigma|F_0|$. [c] $wR_2 = [\Sigma w(F_0^2 - F_c^2)^2/\Sigma w(F_0^2)^2]^{1/2}$; $P = (F_0^2 + 2F_c^2)/3$.

using a He^3 refrigerator. Table 4 summarizes the magnetic properties of $FeGa_2S_4$, $NiGa_2S_4$, $Ni_{0.68}Al_2S_{3.78}$,[32] and structurally similar MAl_2S_4 (M = Mn^{2+}, Fe^{2+}, Co^{2+}) with varying amounts of mixing between M^{2+} and Al^{3+}.

RESULTS AND DISCUSSION

Structure of MAl_2S_4 (M = Mn^{2+}, Fe^{2+}, Co^{2+}). The $MnAl_2S_4$ structure can be described as the hexagonal polymorph (~3 × 36 Å) of the $ZnIn_2S_4$ structure,[14] shown in Figure 2a, with blue spheres representing metal ions in an octahedral environment of S^{2-} ions (yellow spheres) and green spheres representing metal ions in a tetrahedral environment of S^{2-} ions. The MAl_2S_4 (M = Fe^{2+}, Co^{2+}) structure can be described as the trigonal polymorph (~3 × 12 Å) of the $ZnIn_2S_4$ structure, also known as the $FeGa_2S_4$-type structure,[33] shown in Figure 2b, with blue spheres representing metal ions in an octahedral environment (M_{oct}) of S^{2-} ions (yellow spheres) and green spheres representing metal ions in a tetrahedral environment (M_{tet}) of S^{2-} ions. The structure of MAl_2S_4 (M = Mn^{2+}, Fe^{2+}, Co^{2+}) consists of alternating slabs of edge-sharing octahedra that share corners with corner-sharing tetrahedra with every other octahedral slab vacant, which leads to a van der Waals gap. Therefore, MAl_2S_4 (M = Mn^{2+}, Fe^{2+}, Co^{2+}) can be described as 2-d magnets with high two-dimensionality. The blue spheres (octahedral sites) and green spheres (tetrahedral sites) shown in Figure 2 form two planar (2-d), interpenetrating triangular lattices, which can result in frustrated antiferromagnetic coupling of magnetic moments, because of site disorder and geometrical frustration.

Structure of $MnAl_2S_4$. Although the $ZnIn_2S_4$-type $MnAl_2S_4$ polymorph has been previously reported from powder XRD measurements, here, we report, for the first time, the full structure determination and magnetic properties of $ZnIn_2S_4$-type $MnAl_2S_4$.[34] The structure of $MnAl_2S_4$ exhibits mixing of Mn^{2+} and Al^{3+} on both the octahedral and tetrahedral sites. The octahedral sites are occupied by 56% Al^{3+} and 44% Mn^{2+} and surrounded by three equidistant (2.492(3) Å) S^{2-} atoms and three equidistant (2.506(3) Å) S^{2-} atoms. The octahedra are compressed along the c-direction with two in-plane angles of 84.46(3)° and 95.89(16)°. There are two crystallographically unique tetrahedral sites: M1 and M2. The M1 tetrahedral site is occupied by 78% Al^{3+} and 22% Mn^{2+}, and the M2 site is occupied by 68% Al^{3+} and 32% Mn^{2+}. Both tetrahedra are elongated along the c-direction and have apical M1/M2−S^{2-} bonds (2.300(6) Å) that are slightly longer than the remaining three M1/M2−S^{2-} bonds (2.295(3) Å). The bond angles for the M1 tetrahedra are (S^{2-}−M1−S^{2-}) of 112.56(16)° and 106.21(18)°, and the bond angles for the M2 tetrahedra (S^{2-}−M2−S^{2-}) 107.51(17)° and 11.37(16)°. The observed bond distances of M−S^{2-} in the octahedra, where M = Mn^{2+} + Al^{3+}, are intermediate between high-spin, six-coordinate Mn^{2+}−S^{2-} (2.67 Å) and six-coordinate Al^{3+}−S^{2-} (2.38 Å).[35] The observed bond distances of M−S^{2-} in the tetrahedra, where

Table 2. Positional and Atomic Displacement Parameters of MAl_2S_4 (M = Mn^{2+}, Fe^{2+}, Co^{2+}, Ni^{2+}[a])

atom			x	y	z	occupancy	U_{eq} (Å^2)[b]
$MnAl_2S_4$, 150 K							
M1	3*a*	(Mn1 (22(1)%) + Al1 (78(1)%))	0	0	0.60228(11)	1.00	0.0129(12)
M2	3*a*	(Mn2 (32(2)%) + Al2 (68(2)%))	0	0	0.07142(9)	1.00	0.0131(12)
M3	3*a*	(Mn3 (43(2)%) + Al3 (57(2)%))	0	0	0.83723(15)	1.00	0.0133(3)
S1	3*a*		0	0	0.95996(12)	1.00	0.0207(14)
S2	3*a*		0	0	0.71512(11)	1.00	0.0174(14)
S3	3*a*		0	0	0.53910(9)	1.00	0.0175(14)
S4	3*a*		0	0	0.13459(11)	1.00	0.0162(12)
$FeAl_2S_4$, 150 K							
M1	**1*b***	(Fe1 (50(2)%) + Al1 (50(2)%))	0	0	0.5	1.00	0.0280(13)
M2	2*d*	(Fe2 (25(2)%) + Al2 (75(2)%))	$^1/_3$	$^2/_3$	0.7933(3)	1.00	0.0250(12)
S1	2*d*		$^1/_3$	$^2/_3$	0.1336(3)	1.00	0.0275(12)
S2	2*d*		$^1/_3$	$^2/_3$	0.6058(3)	1.00	0.0266(12)
$CoAl_2S_4$, 150 K							
M1	**1*b***	(Co1 (40(2)%) + Al1 (60(2)%))	0	0	0.5	1.00	0.0072(4)
M2	2*d*	(Co2 (30(1)%) + Al2 (70(1)%))	$^1/_3$	$^2/_3$	0.20719(9)	1.00	0.0075(4)
S1	2*d*		$^1/_3$	$^2/_3$	0.86581(8)	1.00	0.0078(4)
S2	2*d*		$^1/_3$	$^2/_3$	0.39502(11)	1.00	0.0076(4)
$Ni_{0.68}Al_2S_{3.78}$,[a] 150 K							
Ni1	**1*b***		0	0	0.5	0.66(3)	0.0136(15)
Al1	2*d*		$^1/_3$	$^2/_3$	0.2090(4)	1.00	0.0151(16)
S1	2*d*		$^1/_3$	$^2/_3$	0.8648(4)	1.00	0.0174(15)
S2	2*d*		$^1/_3$	$^2/_3$	0.3955(3)	0.89(3)	0.0104(14)

[a] $NiAl_2S_4 = Ni_{0.68}Al_2S_{3.78}$. Data taken from ref 32. [b] U_{eq} is defined at one-third of the trace of the orthogonalized U_{ij} tensor.

Table 3. Bond Distances of MAl_2S_4 (M = Mn^{2+}, Fe^{2+}, Co^{2+}, Ni^{2+})

	$MnAl_2S_4$[a]		$FeAl_2S_4$[b]		$CoAlS_4$[c]		$NiAl_2S_4$[d]	
	bond distance (Å)		bond distance (Å)		bond distance (Å)		bond distance (Å)	
Octahedra	M3−S3 (×3)	2.492(3)	M1−S2 (×6)	2.487(2)	M1−S2 (×6)	2.4387(9)	Ni1−S2 (×6)	2.430(2)
	M3−S4 (×3)	2.506(3)						
Tetrahedra								
	M1−S3 (×1)	2.302(7)	M2−S1 (×3)	2.304(8)	M2−S1 (×3)	2.2653(9)	Al1−S1 (×3)	2.264(2)
	M1−S1 (×3)	2.314(3)	M2−S2 (×1)	2.286(5)	M2−S2 (×3)	2.48(2)	Al1−S2 (×1)	2.230(6)
	M2−S4 (×1)	2.300(6)						
	M2−S2 (×3)	2.295(3)						

[a] M = Mn + Al. [b] M = Fe + Al. [c] M = Co + Al. [d] $NiAl_2S_4 = Ni_{0.68}Al_2S_{3.78}$. Data taken from ref 32.

M = Mn^{2+} + Al^{3+} of this phase are intermediate between high-spin, four-coordinate Mn^{2+}−S^{2-} (2.50 Å) and four-coordinate Al^{3+}−S^{2-} (2.23 Å).[35]

Structure of $FeAl_2S_4$. Replacing Ga^{3+} with Al^{3+} in $FeAl_2S_4$ results in a mixing of Fe^{2+} and Al^{3+} on both the octahedral and tetrahedral sites. The octahedral sites M_{oct} (blue spheres in Figure 2b) are occupied by 50% Fe^{2+} and 50% Al^{3+} and surrounded by six equidistant (2.487(2) Å) S^{2-} atoms. These octahedra are compressed along the (111) direction, so there are two in-plane angles 95.54(10)° and 84.46(10)°. The observed bond distances of M_{oct}−S^{2-}, where M = Fe^{2+} and Al^{3+} (2.487(2) Å), are intermediate between that of high-spin, six-coordinate Fe^{2+}−S^{2-} (2.62 Å) and six-coordinate Al^{3+}−S^{2-} (2.38 Å). The tetrahedral sites M_{tet} (the green spheres in Figure 2b) are occupied by 25% Fe^{2+} and 75% Al^{3+} with the apical M_{tet}−S^{2-} bond (2.286(5) Å) slightly shorter than the remaining three M_{tet}−S^{2-} bonds (2.305(2) Å). These tetrahedra are compressed along the *c*-direction with angles of 106.00(10)° and 112.75(10)°. The observed bond distances of M_{tet}−S^{2-}, where M = Fe^{2+} + Al^{3+} (2.286(5)−2.304(8) Å), are intermediate between high-spin, four-coordinate Fe^{2+}−S^{2-} (2.46 Å) and four-coordinate Al^{3+}−S^{2-} (2.23 Å).[35]

Although isotypic $CoGa_2S_4$ and $MnGa_2S_4$ phases have not been reported, the structural effects of replacing Ga^{3+} with Al^{3+} can be investigated by comparing the isostructural $FeGa_2S_4$ and $FeAl_2S_4$. The mixing of Fe^{2+} with Al^{3+} in $FeAl_2S_4$ coincides with a larger unit cell than that expected for substitution without mixing of Al^{3+} for Ga^{3+} in $FeGa_2S_4$ and results in distorted polyhedra. The bond angles of the octahedra (95.54(10)° and

dx.doi.org/10.1021/cm200561p |*Chem. Mater.* 2011, 23, 3086–3094

Table 4. Magnetic Properties of MAl_2S_4 (M = Mn^{2+}, Fe^{2+}, Co^{2+}, Ni^{2+}[a]), $FeGa_2S_4$, and $NiGa_2S_4$

phase		T^* (K)	θ_W (K)	$\lvert\theta_W\rvert/T^*$	ρ_{theo} (μ_B)	ρ_{eff} (μ_B)
$MnAl_2S_4$	(*ab*)	< 1.8	−170	>94.4	5.91 ($S = {}^5/_2$)	5.97
$MnAl_2S_4$	(*c*)	2.5	−160	64.0	5.91	5.95
$FeAl_2S_4$	(*ab*)	10.5	−225	21.4	4.9 ($S = 2$)	5.28
$FeAl_2S_4$	(*c*)	10.5	−225	21.4	4.9	5.33
$CoAl_2S_4$	(*ab*)	5	−234	46.8	3.87 ($S = {}^3/_2$)	4.4
$CoAl_2S_4$	(*c*)	5	−280	56.0	3.87	4.5
$NiAl_2S_4$[a]	(*ab*)	4	−55	13.7	2.83 ($S = 1$)	2.56
$NiAl_2S_4$ (c)[a]		4	−56	14.0	2.83	2.45
$NiGa_2S_4$[b]		8.5	−80	9.4	2.83 ($S = 1$)	2.82
$FeGa_2S_4$[c]		16	−160	10.0	4.9 ($S = 2$)	5.45

[a] $NiAl_2S_4 = Ni_{0.68}Al_2S_{3.78}$. Data taken from ref 32. [b] Data taken from ref 4. [c] Data taken from ref 18.

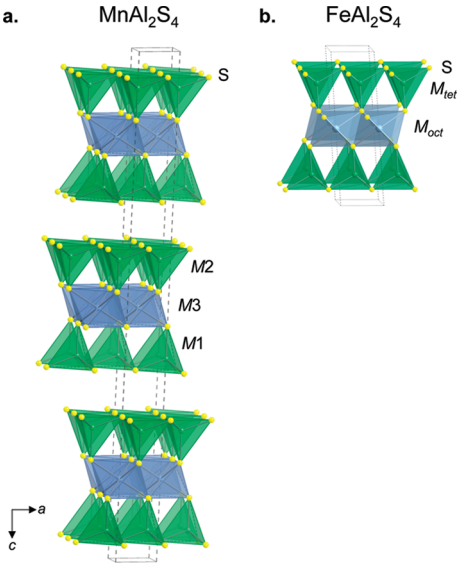

Figure 2. (a) Crystal structure of $MnAl_2S_4$, with M1, M2, and M3 representing $Mn^{2+} + Al^{3+}$. (b) Crystal structure of $FeAl_2S_4$, with M = $Fe^{2+} + Al^{3+}$ and yellow spheres representing S^{2-} ions.

84.46(10)°) in $FeAl_2S_4$ indicate that the octahedra are slightly more compressed (~0.3% more distorted) along the (111) direction, compared with the equivalent bond angles in $FeGa_2S_4$ (95.16(10)° and 84.83(10)°).[13] The bond angles of the tetrahedra (112.75(10)° and 106.00(10)°) in $FeAl_2S_4$ indicate that the tetrahedra are less distorted (~1.3% and ~1.5%, respectively) along the *c*-direction, compared to the equivalent bond angles in in $FeGa_2S_4$ (114.18(10)° and 104.36(10)°).[13]

Structure of $CoAl_2S_4$. Replacing Ga^{3+} with Al^{3+} in $CoAl_2S_4$ results in a mixing of Co^{2+} and Al^{3+} on both the octahedral and tetrahedral sites. The octahedral sites M_{oct} (the blue spheres in Figure 2b) are occupied by 37% Co^{2+} and 63% Al^{3+} and surrounded by six equidistant (2.4388(9) Å) S^{2-} atoms. These octahedra are compressed along the (111) direction, so there are two in-plane angles: 95.83(4)° and 84.17(4)°. The observed bond distance of $M_{oct}-S^{2-}$, where M = Co^{2+} and Al^{3+} (2.4388(9) Å), are intermediate between high-spin, six-coordinate $Co^{2+}-S^{2-}$ (2.59 Å) and six-coordinate $Al^{3+}-S^{2-}$ (2.38 Å).[35] The tetrahedral sites M_{tet} (the green spheres in Figure 2b) are occupied by 29% Co^{2+} and 71% Al^{3+} with the apical $M_{tet}-S^{2-}$ bond (2.248(2) Å) being slightly shorter than the remaining three $M_{tet}-S^{2-}$ bonds (2.654(9) Å). These tetrahedra are compressed along the *c*-direction. The observed bond distances of $M_{tet}-S^{2-}$, where M = Co^{2+} + Al^{3+}, are intermediate between high-spin, four-coordinate $Co^{2+}-S^{2-}$ (2.42 Å) and four-coordinate $Al^{3+}-S^{2-}$ (2.23 Å).[35]

Physical Properties of $MnAl_2S_4$. Figure 3a shows the temperature dependence of the magnetic susceptibility of $MnAl_2S_4$ under 0.01 and 5 T. Bifurcation at the spin freezing temperature, T^* = 2.5 K, between zero-field-cooled (ZFC) and field-cooled (FC) measurements at 0.01 T for B // c and is suppressed with increasing applied field. This spin-freezing behavior is characteristic for a spin glass system with site disorder by mixing of Mn^{2+} and Al^{3+} ions at both the octahedral and tetrahedral sites. However, for B // ab, no hysteresis is observed down to 1.8 K, and T^* should be observed at T < 1.8 K. The hysteresis disappears with applied field. The magnetic susceptibility data were fit by the Curie−Weiss law, $\chi = C/(T - \theta_W)$, for T > 150 K for all analogues, and the estimated Weiss temperature (θ_W) and effective moment (p_{eff}) values are listed in Table 4. The value of p_{eff} is estimated to be 5.95 μ_B for B // c and 5.97 μ_B for B // ab, which is consistent with the theoretical value for $S = {}^5/_2$ (p_{theo} = 5.92 μ_B). With high-spin Mn^{2+} ions located at the octahedral ($(t_{2g})^3(e_g)^2$) and tetrahedral ($(e)^2(t_2)^3$) sites, $MnAl_2S_4$ can be regarded as a $S = {}^5/_2$ Heisenberg antiferromagnet with no orbital order. The ratio of susceptibility of χ_c/χ_{ab}, as a function of T under 5 T, is ~1 down to 2 K, as shown in the inset of Figure 3a, which indicates that this is an approximate 2-d Heisenberg system. The frustration parameter $\lvert\theta_W\rvert/T^* \approx 64$ for B // c is large, which can be attributed primarily to strong site disorder, two-dimensionality, and the isotropic Heisenberg nature of the Mn^{2+} spins, with geometrical frustration of both the octahedral (the blue spheres in Figure 2) and tetrahedral (the green spheres in Figure 2) sublattices also playing a role.

Figure 3b shows the total specific heat C_p/T as a function of T in various fields. Unlike the structurally similar Ga-analogues, $MnGa_2S_4$, which order at low temperature (below 20 K), no magnetic long-range order is observed down to 0.4 K in $MnAl_2S_4$. Because of the lack of a nonmagnetic analogue with the same crystal structure, the magnetic specific heat of MAl_2S_4 (M = Mn, Fe, Co) has not been determined. Development of short-range magnetic correlations is observed as a shallow broad maximum at $T \approx 2$ K. The absence of long-range magnetic ordering is characteristic for spin-glass systems. C_p/T exhibits a broad feature at T = 80 K, which may be attributed to the incoherent moment-free spin clusters. An upturn of C_p/T below 0.5 K is attributable to the nuclear quadrupole specific heat (C_{nq}).

dx.doi.org/10.1021/cm200561p |*Chem. Mater.* 2011, 23, 3086–3094

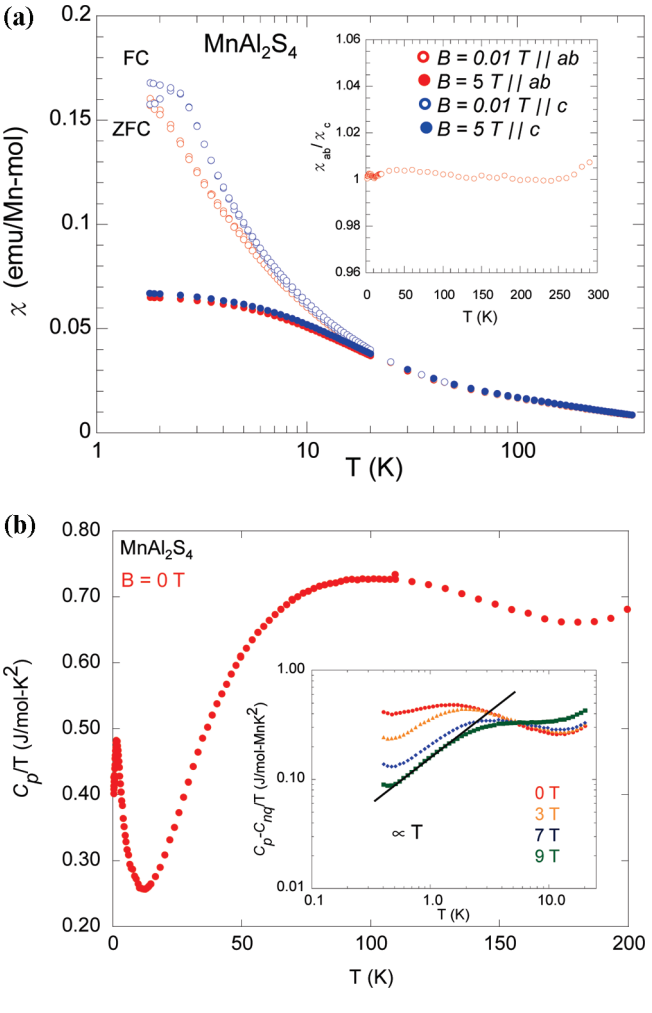

Figure 3. (a) ZFC and FC temperature-dependent magnetic susceptibility of $MnAl_2S_4$ at 0.01 and 5 T along both the *ab*-plane and the *c*-axis. The inset shows χ_{ab}/χ_c as a function of *T*. (b) The total specific heat C_p/T is shown as a function of *T* at 0 T. The inset shows $(C_p - C_{nq})/T$ plotted as a function of *T* at applied fields of 0, 3, 7, and 9 T along the *c*-axis.

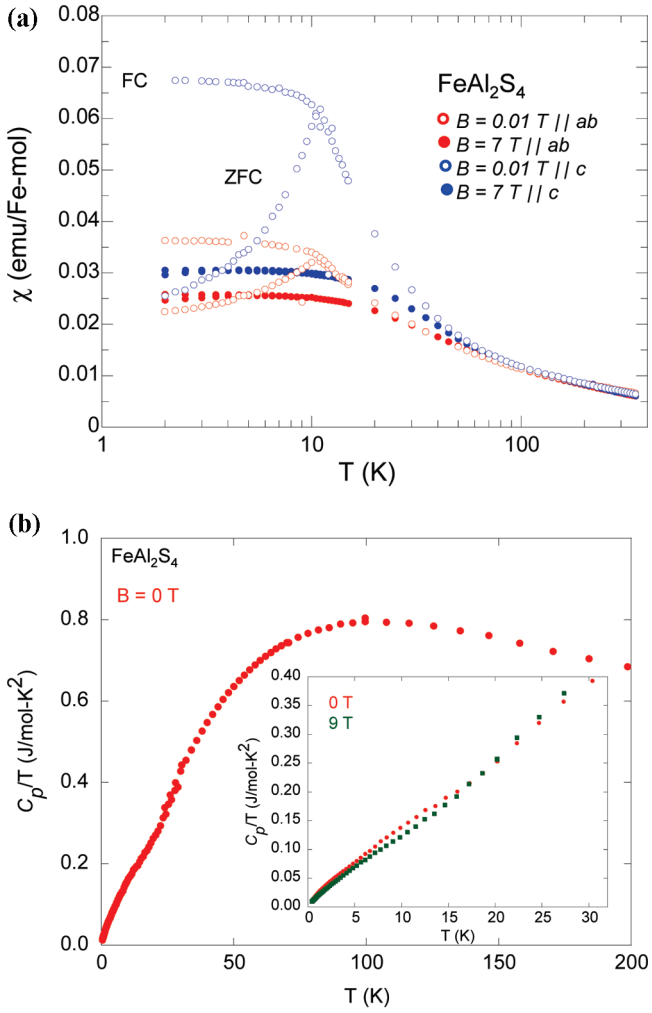

Figure 4. (a) ZFC and FC temperature-dependent magnetic susceptibility of $FeAl_2S_4$ at 0.01 and 7 T along both the *ab*-plane and *c*-axis. (b) The total specific heat, C_p/T, as a function of *T* is plotted at 0 T. The inset shows the low-temperature data between 0.04 K and 30 K at 0 and 9 T along the *c*-axis.

C_{nq} can be estimated to be $8.31 \times 10^{-4}/T^2$ (J/(mol K)) at 0 T and was subtracted from C_p to show $(C_p - C_{nq})/T$ in the inset of Figure 3b.[16] $(C_p - C_{nq})/T$ is almost constant at 0 T, while $(C_p - C_{nq})/T$ is suppressed at low temperatures under applied field along the *c*-axis. Generally, for spin-glass systems, magnetic specific heat shows *T*-linear dependence, because of a broad continuous distribution in energy of the spin excitations. However, the application of magnetic field should open the gap in the spin excitations and suppress $(C_p - C_{nq})/T$ at $T \rightarrow 0$ K.

Physical Properties of $FeAl_2S_4$. Figure 4a shows the temperature dependence of the magnetic susceptibility of $FeAl_2S_4$ at 0.01 and 7 T. Bifurcation at the spin freezing temperature, $T^* = 10.5$ K, between ZFC and FC measurements for $B // ab$ and *c* is observed, with site disorder by mixing of Fe^{2+} and Al^{3+} ions. The estimated effective moment (p_{eff}) and Weiss temperature (θ_W) by Curie–Weiss fitting above 150 K are shown in Table 4. The effective moment (p_{eff}) for $FeGa_2S_4$ is 5.71 μ_B and the anisotropic effective moments for $FeAl_2S_4$ are 5.28 μ_B in the *ab*-plane and 5.33 μ_B along the *c*-axis. The calculated effective magnetic moments are larger than the spin-only theoretical value ($p_{theo} = 4.90\ \mu_B$), due to spin–orbital coupling of the Fe^{2+} ions on both the octahedral and tetrahedral sites . This is consistent with the fact that Fe^{2+} has $S = 2$ spins on both the octahedral ($(t_{2g})^4(e_g)^2$) and tetrahedral ($(e)^3(t_2)^3$) sites, thus $FeAl_2S_4$ can be regarded as an $S = 2$ system as well as $FeGa_2S_4$. χ_c/χ_{ab} is enhanced below ~90 K, which indicates $FeAl_2S_4$ has easy-axis anisotropy that can also be attributed to the spin–orbital interaction. The frustration parameter $|\theta_W|/T^* \sim 21$ for $B // c$ and $B // ab$ is large, which can be attributed primarily to strong site disorder and two-dimensionality, with geometrical frustration of both the octahedral (blue spheres in Figure 2) and tetrahedral (green spheres in Figure 2) sublattices also playing a role.

$FeAl_2S_4$ can be described as isostructural to $FeGa_2S_4$ but nominally more frustrated with a freezing temperature (T^*) of 10.5 K, compared to 16 K for $FeGa_2S_4$ and a θ_W value of −225 K, compared to −160 K for $FeGa_2S_4$. The weak magnetic anisotropy in $FeAl_2S_4$ can be attributed to the distribution of Fe^{2+} atoms in both octahedral and tetrahedral sites of $FeAl_2S_4$, which is similar to the almost-isotropic behavior observed in the Ga-analogue, $FeGa_2S_4$.[23]

dx.doi.org/10.1021/cm200561p |*Chem. Mater.* 2011, 23, 3086–3094

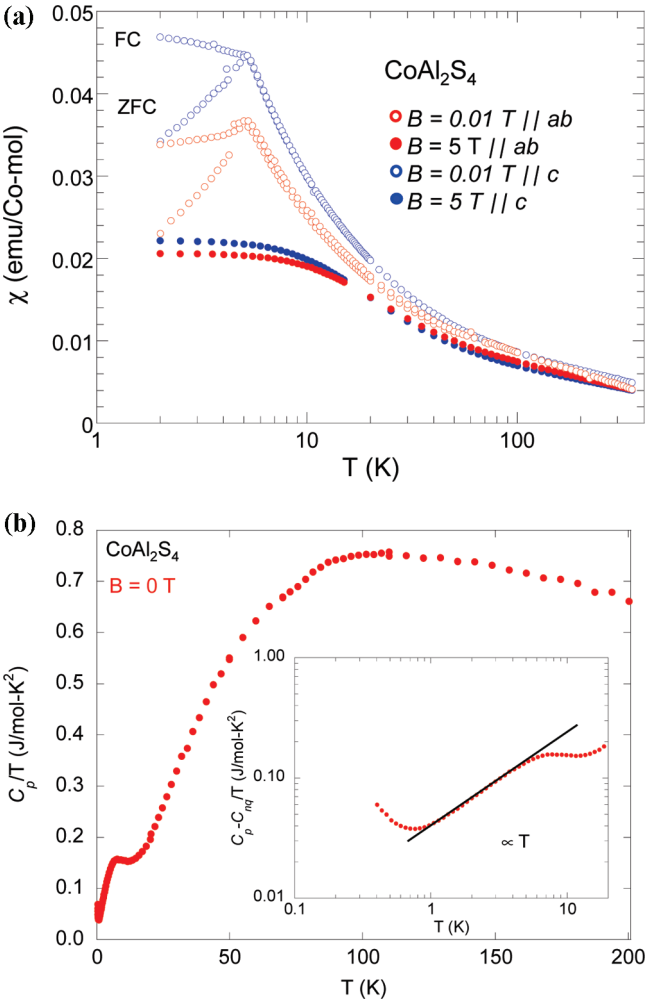

Figure 5. (a) ZFC and FC temperature-dependent magnetic susceptibility of $CoAl_2S_4$ at 0.01 and 5 T along both the *ab*-plane and the *c*-axis. (b) The total specific heat, $(C_p - C_{nq})/T$, is plotted as a function of T at 0 T. The inset shows the low-temperature data (0.04−20 K) at 0 T.

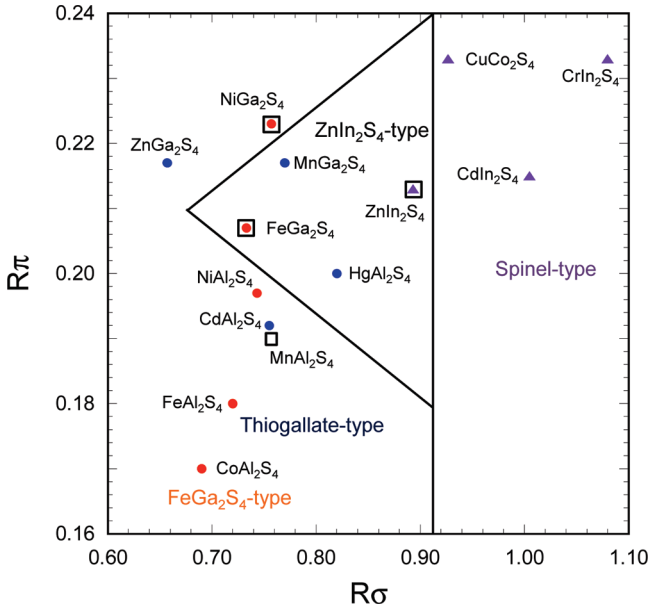

Figure 6. A segment of the structure field map for AB_2S_4 compounds (where A is a transition metal and B is a transition metal or main group metal) compiled by Haeuseler is shown with the $FeGa_2S_4$-type structures (represented by orange spheres), $ZnIn_2S_4$-type structures (represented by black squares), thiogallate-type structures (represented by blue spheres), and spinel-type structures (represented by green spheres). The lines indicate the calculated border between structure types, as determined by Haeuseler.[42]

Figure 4b shows the total specific heat (C_p/T), as a function of T. No magnetic ordering is observed down to 0.4 K. There is a weak shoulder peak at ∼10 K close to the freezing temperature (T^* = 10.5 K), which is also found in other MGa_2S_4 (M = Fe, Ni) compounds.[4,18] This suggests that the spin excitation spectrum of $FeAl_2S_4$ has a linear dispersion characteristic to 2-d antiferromagnetism, not the continuous distribution that is expected for canonical spin-glass systems. C_p shows almost T^2-dependence even at 9 T, and $FeAl_2S_4$ shows no field dependence, as seen in the inset of Figure 4b.

Physical Properties of $CoAl_2S_4$. Figure 5a shows the temperature-dependent magnetic susceptibility at 0.01 and 5 T. Hysteresis between ZFC and FC measurements is observed at T^* = 5 K, which is characteristic behavior in spin-glass systems. We fit the data to Curie−Weiss law for T above 150 K, and the estimated p_{eff} and θ_W values are listed in Table 4. An observed p_{eff} value of 4.4 μ_B is larger than the theoretical spin-only value (p_{theo} = 3.87 μ_B), and the larger moment of Co^{2+} can be attributed to spin−orbital coupling in a tetrahedral environment. This has been observed in $Co_{0.11}Zn_{0.89}O$, $CoAl_2O_4$, $Co_{0.20}Zn_{0.80}Al_2O_4$, $Co_{0.20}Mg_{0.80}Al_2O_4$, and $CoAl_{2-x}Ga_xO_4$.[25,36] The temperature dependence of χ_c/χ_{ab} at 5 T is enhanced below ∼50 K, which indicates easy-axis anisotropy, similar to $FeAl_2S_4$, and is attributable to spin−orbital interaction on the octahedral site. Although Co^{2+} ions are located on the octahedral ($(t_{2g})^5(e_g)^2$) and tetrahedral ($(e)^3(t_2)^4$), $CoAl_2S_4$ can be regarded as a $S = {}^3/_2$ system. The large frustration parameter $|\theta_W|/T^* \approx 46$ for B // c can be attributed to the combination of strong site disorder and two-dimensionality, with geometrical frustration also playing a role.

Figure 5b shows the total specific heat C_p/T as a function of T at 0 T. Similar to γ-$CoGa_2S_4$, $CoAl_2S_4$ shows no magnetic phase transitions, which correspond to the formation of long-range order down to 0.4 K. C_p exhibits a broad peak at ∼6.5 K, which are close to the freezing temperature (T^* = 5 K) found in other MAl_2S_4 compounds, such as MGa_2S_4 (M = Fe^{2+}, Ni^{2+}) compounds,[4,18] which can be attributed to the development of short-range magnetic ordering below 6.5 K. An upturn of C_p/T below 0.5 K is attributable to nuclear quadrupole specific heat (C_{nq}). C_{nq} is estimated as $6.11 \times 10^{-4}/T^2$ (J/(mol K)) at 0 T. The inset of Figure 5b shows the temperature dependence of $(C_p - C_{nq})/T$. Consistent with the spin freezing behavior observed in susceptibility at 0.01 T, $(C_p - C_{nq})/T$ has a finite value at the lowest temperature limit. This suggests that the spin excitation spectrum of $CoAl_2S_4$, similar to $MnAl_2S_4$, has the continuous distribution expected for spin-glass systems.

Comparison of MAl_2S_4 (M = Mn^{2+}, Fe^{2+}, Co^{2+}), $Ni_{0.68}Al_2S_{3.78}$, $FeGa_2S_4$, and $NiGa_2S_4$. The MGa_2S_4 (M = Mn^{2+}, Fe^{2+}, Co^{2+}, Ni^{2+}) phases are structurally related with the MAl_2S_4 (M = Mn^{2+}, Fe^{2+}, Co^{2+}) and $Ni_{0.68}Al_2S_{3.78}$ phases, since all are built of the same structural moieties, edge-sharing octahedra that share corners with corner-sharing tetrahedra. The magnetic frustration exhibited by MGa_2S_4 can be attributed to a combination of the geometrical frustration due to the antiferromagnetic correlations

dx.doi.org/10.1021/cm200561p |*Chem. Mater.* 2011, 23, 3086–3094

of M^{2+} (M^{2+} = Fe^{2+}, Ni^{2+}) moments on a triangular sublattice and the 2-d magnetic lattice due to the absence of every other octahedral slab. The magnetic behavior of MAl_2S_4 is significantly more complicated with mixing of M^{2+} and Al^{3+} in two triangular sublattices: the octahedral and tetrahedral sublattices. The mixing of M^{2+} and Al^{3+} in the MAl_2S_4 results in weak magnetic anisotropy, which increases the effective dimensionality of the MAl_2S_4 and also serves to heighten the effects of site disorder as compared to geometrical frustration and low dimensionality. The magnetic behavior of the structurally ordered MGa_2S_4 (M = Fe^{2+}, Ni^{2+}) phases can be used to estimate the effects of site disorder on magnetic correlations in MAl_2S_4 (M = Mn, Fe, Co), thereby isolating the geometrical frustration and dimensionality parameters from the site disorder parameter in these structurally related phases. Here, we see that magnetic frustration increases with the addition of site disorder in MAl_2S_4 (M = Fe^{2+}, Ni^{2+}), because of either mixing of Fe^{2+} and Al^{3+} in $FeAl_2S_4$ or the partial occupancy of Ni^{2+} and S^{2-} in $Ni_{0.68}Al_2S_{3.78}$,[32] by roughly ~55% and ~31%, respectively, compared to the structurally ordered MGa_2S_4 (M = Fe^{2+}, Ni^{2+}) phases. The frustration across the MAl_2S_4 series (M = Mn^{2+}, Fe^{2+}, Co^{2+}), as indicated by the frustration parameter ($|\theta_W|/T^*$), also increases with increasing structural distortion, as evidenced by the increase in distortion in both the tetrahedral and octahedral environments with decreasing ionic M^{2+} radius. The additional magnetic frustration in MAl_2S_4, compared to MGa_2S_4, can be attributed to the inhomogeneous environment surrounding the magnetic moments, similar to the spin-glass behavior in $CoAl_{2-x}Ga_xO_4$.[25]

CONCLUSIONS

No long-range magnetic ordering was observed down to 0.4 K for MAl_2S_4 (M = Mn^{2+}, Fe^{2+}, Co^{2+}). Instead, we observed bifurcation between ZFC and FC measurements below the spin freezing temperature (T^*) in magnetic susceptibility of MAl_2S_4 (M = Mn^{2+}, Fe^{2+}, Co^{2+}), which is characteristic of spin-glass systems. The spin-glass behavior seen at 0.1 T is suppressed with increasing applied field and completely disappears at 5 or 7 T. A broad peak in C_p below T^* is attributable to the development of short-range order.

Both $MnAl_2S_4$ ($S = {}^5/_2$) and $CoAl_2S_4$ ($S = {}^3/_2$) show spin-glass behavior below T^* in ZFC and FC susceptibility measurements at 0 T, also show $C_p \propto T$ and exhibit nuclear quadrupole interactions at low temperature, whereas $FeAl_2S_4$ does not exhibit nuclear quadrupole interactions at low temperature in the heat capacity. In particular, the frustration parameters $|\theta_W|/T^*$ are large for $MnAl_2S_4$ and $CoAl_2S_4$. Theoretically, the two-dimensional (2-d) Heisenberg spin-glass system is not expected to show any spin freezing at finite temperature. The almost-Heisenberg (isotropic) nature of Mn^{2+} ($S = {}^5/_2$) spins, strong site disorder, and two-dimensionality should be the origin of the strong suppression of the spin-glass freezing.

For $FeAl_2S_4$ ($S = 2$), C_p exhibits T^2-dependence originating from 2-d linear dispersion with almost no difference in low-temperature C_p value between 0 and 9 T. This is different from the typical T-linear dependence characteristic of spin glasses seen in the Mn- and Co-analogues. This T^2-dependence of C_p also supports previous results on the impurity effects on $NiGa_2S_4$, which indicate that the integer size of the Heisenberg spins is important to stabilize the 2-d spin wave-like coherent behavior.[16] The origin of this behavior is not clear at this point, and possible candidates include a spin nematic[37−40] and a Z_2-vortex transition that is due to the novel magnetic phase.[41] Future studies involve microscopic magnetic structure determination by neutron diffraction studies.

A possible explanation for the previously unreported Fe^{2+}-, Co^{2+}-, and Ni^{2+}- analogues is the fact that these compounds lie on the edge of structural stability of the MAl_2S_4 phase (where M is a divalent metal). One obvious reason is the decrease in size from Mn^{2+} to Ni^{2+}. When comparing the tetrahedral angles and octahedral angles as a function of ionic radii, the distortion in both the tetrahedral and octahedral environments decrease as the ionic radii increase. The decrease in size of M^{2+} (M^{2+} = Mn^{2+}, Fe^{2+}, Co^{2+}, and Ni^{2+}) across the series coincides with change in disorder type from a mixing of M^{2+}/Al^{3+} at the octahedral and tetrahedral sites in MAl_2S_4 (M = Mn^{2+}, Fe^{2+}, Co^{2+}) to partial occupancy of Ni^{2+} and S^{2-} in $Ni_{0.68}Al_2S_{3.78}$.[32] This is also consistent with the increasing frustration parameter that is observed with decreasing ionic M^{2+} radius.

To rationalize the structural differences between MAl_2S_4 (M = Mn^{2+}, Fe^{2+}, Co^{2+}, and Ni^{2+}) compounds, we have consulted structure field maps. The structure field maps compiled using mean values of pseudo-potential radii by Haeuseler have been used to successfully predict new compounds of the various $ZnIn_2S_4$-polytypes and to also explain the absence of others.[42] We have included several compounds that adopt the $FeGa_2S_4$-type structure, using the map compiled by Haeuseler in Figure 6. The separation between the $ZnIn_2S_4$-type and thiogallate-type structures, as well as the separation between the $ZnIn_2S_4$-type and $FeGa_2S_4$-type structures, is good, but the separation between the thiogallate-type and the $FeGa_2S_4$-type structures is not well-resolved. The $FeGa_2S_4$-type MAl_2S_4 (M = Fe^{2+}, Co^{2+}, Ni^{2+}) and $MnAl_2S_4$ ($ZnIn_2S_4$-type) compounds are close to the border separating the $FeGa_2S_4$-type and $ZnIn_2S_4$-type structures. Similar observations have been used to rationalize the lack of compounds of MGa_2S_4−MCr_2S_4 (M = Zn, Cd, Hg) with the $ZnIn_2S_4$-type structure,[42] can explain the previous failed attempts to grow these compounds,[15] and this is consistent with increased structural instability upon moving across the series, from Mn^{2+} to Ni^{2+}.

ASSOCIATED CONTENT

Supporting Information. Crystallographic information files (CIF). This material is available free of charge via the Internet at http://pubs.acs.org.

AUTHOR INFORMATION

Corresponding Author
*Tel.: +1-225-578-2695 Fax: +1-225-578-3458. E-mail: jchan@lsu.edu.

ACKNOWLEDGMENT

M.C.M. acknowledges Dr. F. R. Fronczek for useful discussions. M.C.M. and J.Y.C. acknowledge NSF Grant No. DMR 0756281 and 1063735 for partial support of this project. This work was partially supported by Grant-in-Aid (No. 20340089, No. 21684019) from the Japanese Society for the Promotion of Science, and also Grant-in Aid for Scientific Research on Priority Area (No. 19052003, No.1702005) from the Ministry of Education, Culture, Sports, Science and Technology, Japan. R.I. acknowledges the Global COE Program "The Physical Sciences Frontier", MEXT, Japan. ALS is supported by the U.S.

Department of Energy, Office of Energy Sciences Materials Sciences Division, under Contract No. DE-AC02-05CH11231.

REFERENCES

(1) Moessner, R.; Ramirez, A. P. *Phys. Today* **2006**, *2006*, 24–29.
(2) Greedan, J. E. *J. Alloys Compd.* **2006**, *408*−*412*, 444–455.
(3) Levi, B. G. *Phys. Today* **2007**, *2007*, 16–19.
(4) Nakatsuji, S.; Nambu, Y.; Tonomura, H.; Sakai, O.; Jonas, S.; Broholm, C.; Tsunetsugu, H.; Qiu, Y.; Maeno, Y. *Science* **2005**, *309*, 1697–1700.
(5) Affleck, J. *J. Phys.: Condens. Matter* **1989**, *1*, 3047.
(6) Collins, M. F.; Petrenko, O. A. *Can. J. Phys.* **1997**, *75*, 605–655.
(7) Nakatsuji, S.; Nambu, Y.; Onoda, S. *J. Phys. Soc. Jpn.* **2010**, *79*, 011003.
(8) Radaelli, P. G.; Horibe, Y.; Gutmann, M. J.; Ishibashi, H.; Chen, C. H.; Ibberson, R. M.; Koyama, Y.; Hor, Y.-S.; Kiryukhin, V.; Cheong, S.-W. *Nature* **2002**, *416*, 155–158.
(9) Schmidt, M.; Ratcliff, W.; Radaelli, P. G.; Refson, K.; Harrison, N. M.; Cheong, S. W. *Phys. Rev. Lett.* **2004**, *92*, 056402.
(10) Fritsch, V. *Phys. Rev. Lett.* **2004**, *92*, 116401.
(11) Hemberger, J.; Lunkenheimer, P.; Fichtl, R.; Krug von Nidda, H. A.; Tsurkan, V.; Loidl, A. *Nature* **2005**, *434*, 364–367.
(12) Weber, S.; Lunkenheimer, P.; Fichtl, R.; Hemberger, J.; Tsurkan, V.; Loidl, A. *Phys. Rev. Lett.* **2006**, *96*, 157202.
(13) Dogguy Smiri, L.; Dung, N. H.; Pardo, M. P. *Mater. Res. Bull.* **1980**, *15*, 861–866.
(14) Lappe, F.; Niggli, A.; Nitsche, R.; White, J. G. *Z. Kristallogr.* **1962**, *117*, 146–152.
(15) Chaus, I. S.; Sheka, I. A. *Russ. Chem. Rev.* **1969**, *38*, 375–388.
(16) Nambu, Y.; Nakatsuji, S.; Maeno, Y.; Okudzeto, E.; Chan, J. Y. *Phys. Rev. Lett.* **2008**, *101*, 207204.
(17) Myoung, B. R.; Kim, S. J.; Kim, C. S. *J. Korean Phys. Soc.* **2008**, *53*, 750–753.
(18) Nakatsuji, S.; Tonomura, H.; Onuma, K.; Nambu, Y.; Sakai, O.; Maeno, Y.; Macaluso, R. T.; Chan, J. Y. *Phys. Rev. Lett.* **2007**, *99*, 157203.
(19) Tomita, T.; Nambu, Y.; Nakatsuji, S.; Koeda, S.; Hedo, M.; Uwatoko, Y. *J. Phys. Soc. Jpn.* **2009**, *78*, 094603.
(20) Takubo, K.; Mizokawa, T.; Nambu, Y.; Nakatsuji, S. *Phys. Rev. B* **2009**, *79*, 134422.
(21) Rimet, R.; Buder, R.; Schlenker, C. *Solid State Commun.* **1981**, *37*, 693–697.
(22) Pardo, M. P. *Mater. Res. Bull.* **1982**, *17*, 1477–1481.
(23) Agnostinelli, E.; Gastaldi, L.; Viticoli, S. *J. Phys. Chem. Solids* **1985**, *46*, 1345–1349.
(24) Tsuboi, N.; Ogihara, K.; Suda, Y.; Oishi, K.; Kobayashi, S.; Kaneko, F. *Jpn. Soc. Appl. Phys.* **2005**, *44*, 725–728.
(25) Melot, B. C.; Page, K.; Seshadri, R.; Stoudenmire, E. M.; Balents, L.; Bergman, D. L.; Proffen, T. *Phys. Rev. B.* **2009**, *80*, 104420.
(26) Le, M. L. P.; Strobel, P.; Colin, C. V.; Pagnier, T.; Alloin, F. *J. Phys. Chem. Solids* **2011**, *72*, 124–135.
(27) *Bruker SAINT Version 7.6A Software Reference Manual*; Bruker AXS, Inc.: Madison, WI, 2007.
(28) Sheldrick, G. M. *SADABS v2008/1 semi-empirical absorption and beam correction program*, University of Göttingen, Göttingen, Germany, 2008.
(29) Altomare, A.; Burla, M. C.; Camalli, M.; Cascarano, G.; Giacovazzo, C.; Guagliardi, A.; Polidori, G. *J. Appl. Crystallogr.* **1994**, *27*, 435.
(30) Sheldrick, G. M. *Acta Crystallogr., Sect. A: Found Crystallogr.* **2008**, *64A*, 112–122.
(31) Spek, A. L. *J. Appl. Crystallogr.* **2003**, *36*, 7–13.
(32) Higo, T.; Ishii, R.; Menard, M. C.; Chan, J. Y.; Yamaguchi, H.; Hagiwara, M.; Nakatsuji, S. *Phys. Rev. B.* **2011**, in press.
(33) Smiri, D.; Dung, N. H.; Pardo, M. P. *Mater. Res. Bull.* **1980**, *15*, 861–866.
(34) Flahaut, J. *C. R. Acad. Sci. Paris* **1951**, *233*, 1279.
(35) Shannon, R. D.; Prewitt, C. T. *J. Inorg. Nuc. Chem.* **1968**, *30*, 1389–1398.
(36) Cossee, P.; Van Arkel, A. E. *J. Phys. Chem. Solids* **1960**, *15*, 1–6.
(37) Tsunetsugu, T.; Arikawa, M. *J. Phys. Soc. Jpn.* **2006**, *75*, 083701.
(38) Lauchli, A.; Mila, F.; Penc, K. *Phys. Rev. Lett.* **2006**, *97*, 087502.
(39) Bhattacharjee, S.; Shenoy, V. B.; Senthil, T. *Phys. Rev. B* **2006**, *74*, 092406.
(40) Li, P.; Zhang, G. M.; Shen, S. Q. *Phys. Rev. B* **2007**, *75*, 104420.
(41) Kawamura, H.; Miyashita, S. *J. Phys. Soc. Jpn.* **1984**, *53*, 4138–4154.
(42) Haeuseler, H. *J. Solid State Chem.* **1990**, *86*, 275–278.